INL/JOU-13-30373

Advanced Multiphysics Coupling for LWR Fuel Performance Analysis

J. D. Hales, M. R. Tonks, F. N. Gleicher, B. W. Spencer, S. R. Novascone, R. L. Williamson, G. Pastore, D. M. Perez

October 2015

The INL is a
U.S. Department of Energy
National Laboratory
operated by
Battelle Energy Alliance

This document was prepared as an account of work sponsored by an agency of the United States Government. Neither the United States Government nor any agency thereof, or any of their employees, makes any warranty, expressed or implied, or assumes any legal liability or responsibility for any third party's use, or the results of such use, of any information, apparatus, product or process disclosed in this report, or represents that its use by such third party would not infringe privately owned rights. The views expressed in this paper are not necessarily those of the United States Government or the sponsoring agency.

Prepared for the U.S. Department of Energy
Office of Nuclear Energy
Under DOE Idaho Operations Office
Contract DE-AC07-05ID14517

Advanced Multiphysics Coupling for LWR Fuel Performance Analysis

J. D. Hales*, M. R. Tonks, F. N. Gleicher, B. W. Spencer, S. R. Novascone, R. L. Williamson, G. Pastore, D. M. Perez

Fuel Modeling and Simulation, Idaho National Laboratory, P.O. Box 1625, Idaho Falls, ID 83415-3840

Abstract

Even the most basic nuclear fuel analysis is a multiphysics undertaking, as a credible simulation must consider at a minimum coupled heat conduction and mechanical deformation. The need for more realistic fuel modeling under a variety of conditions invariably leads to a desire to include coupling between a more complete set of the physical phenomena influencing fuel behavior, including neutronics, thermal hydraulics, and mechanisms occurring at lower length scales. This paper covers current efforts toward coupled multiphysics LWR fuel modeling in three main areas.

The first area covered in this paper concerns thermomechanical coupling. The interaction of these two physics, particularly related to the feedback effect associated with heat transfer and mechanical contact at the fuel/clad gap, provides numerous computational challenges. An outline is provided of an effective approach used to manage the nonlinearities associated with an evolving gap in BISON, a nuclear fuel performance application.

A second type of multiphysics coupling described here is that of coupling neutronics with thermomechanical LWR fuel performance. DeCART, a high-fidelity core analysis program based on the method of characteristics, has been coupled to BISON. DeCART provides sub-pin level resolution of the multigroup neutron flux, with resonance treatment, during a depletion or a fast transient simulation. Two-way coupling between these codes was achieved by mapping fission rate density and fast neutron flux fields from DeCART to BISON and the temperature field from BISON to DeCART while employing a Picard iterative algorithm.

Finally, the need for multiscale coupling is considered. Fission gas production and evolution significantly impact fuel performance by causing swelling, a reduction in the thermal conductivity, and fission gas release. The mechanisms involved occur at the atomistic and grain scale and are therefore not the domain of a fuel performance code. However, it is possible to use lower lengthscale models such as those used in the mesoscale MARMOT code to compute average properties, e.g. swelling or thermal conductivity. These may then be used by an engineering-scale model. Examples of this type of multiscale, multiphysics modeling are shown.

Keywords: multiphysics, fuel performance analysis

1. Introduction

The computational analysis of nuclear fuel performance is an example of the need for multiphysics simulation capabilities. The phenomena associated with nuclear fuel behavior operate over widely varying time and length scales and are often tightly coupled. A well-known example of coupled behavior is the closure of the fuel-cladding gap in light water reactor fuel rods. The need for improved capabilities has been recently highlighted (Rashid et al., 2011).

The BISON code (Williamson et al., 2012) is under development at Idaho National Laboratory (INL) as a next-generation, multiphysics nuclear fuel performance application. BISON is based on the Multiphysics Object-Oriented Simulation Environment (MOOSE) (Gaston et al., 2009), a massively parallel, finite element-based framework to solve systems of coupled nonlinear partial differential equations using the Jacobian-free Newton Krylov (JFNK) method (Knoll and Keyes, 2004). MOOSE supports the use of one-, two-, and three-dimensional meshes and uses implicit time integration, important for the widely varying time scales in nuclear fuel simulation. An object-oriented architecture is employed, minimizing the programming required to add new material and behavior models. A variety of applications based on MOOSE have been developed for multiphysics modeling of problems in geomechanics, reactive transport, neutronics, crud formation, and other fields.

BISON solves discretized equations of static equilibrium, heat transfer, and heat transfer across a gap to model the fuel-cladding gap in LWR fuel rods. The nonlinear, coupled nature of gap heat transfer can pose numerical difficulties. Section 2 reviews these concepts.

Section 3 discusses strategies for solving multiple physics. A tight coupling approach is shown to be advantageous for thermomechanical nuclear fuel modeling.

One of the features of BISON is its ability to couple to other applications. In one such coupling, BISON is used in conjunc-

*Corresponding author

Email addresses: Jason.Hales@inl.gov (J. D. Hales), Michael.Tonks@inl.gov (M. R. Tonks), Frederick.Gleicher@inl.com (F. N. Gleicher), Benjamin.Spencer@inl.gov (B. W. Spencer), Stephen.Novascone@inl.gov (S. R. Novascone), Richard.Williamson@inl.gov (R. L. Williamson), Giovanni.Pastore@inl.gov (G. Pastore), Danielle.Perez@inl.gov (D. M. Perez)

tion with the DeCART neutronics code (Joo et al., 2004, 2002) to solve both one- and two-way coupled neutron transport and fuels performance problems. DeCART provides BISON pin resolved quantities such as power density, fission rate density, and the fast neutron flux. Since these quantities may be obtained from a detailed assembly calculation, they include the effects of different assembly elements such as control rods and water holes. The effects of these phenomena and reactor characteristics are not normally included in fuel analysis calculations. BISON in turn is able to provide an accurate temperature distribution to DeCART for the pin of interest. DeCART uses this temperature distribution to help calculate cross sections. This coupling of neutronics with thermomechanical fuel performance is the subject of Section 4.

As a third example of multiphysics coupling, the impact of lower lengthscale phenomena on the macro scale fuel performance is considered by coupling to atomic and mesoscale simulation codes. For this coupling, the mesoscale MARMOT code (Tonks et al., 2012), which is also based on the MOOSE framework, is employed. MARMOT predicts the co-evolution of microstructure and properties due to applied load, temperature, and radiation damage. The multiscale coupling is handled in two ways: concurrent coupling in which BISON and MARMOT run simultaneously and pass information back and forth, and hierarchical coupling in which atomistic and mesoscale models are used to develop mechanistic materials models for use in BISON. Section 5 demonstrates both approaches for multiscale simulations of nuclear fuel.

The paper concludes with thoughts about what advantages the next stage of computational multiphysics modeling may provide.

2. Overview of BISON

BISON is a nuclear fuel performance analysis application based on the finite element method. Though primarily used for LWR fuel analysis, BISON has been used to analyze TRISO-coated particle fuel (Hales et al., 2013) and metal fuel in rod and plate form (Medvedev, 2012; Carlson et al., 2013), design and interpret irradiation experiments (Medvedev, 2013), and investigate novel fuel concepts (Metzger et al., 2014).

BISON solves the coupled equations of stress equilibrium and heat conduction, and, optionally, species diffusion. Because it uses the finite element method to solve these equations on an arbitrary mesh, it can be used to analyze a variety of thermomechanical problems that may or may not be associated with nuclear fuel. These equations are typically solved simultaneously (tight coupling).

When analyzing nuclear fuel, BISON employs models for fuel densification and swelling, fuel relocation, cladding creep, fission gas generation and release, mechanical fuel/cladding contact, gap heat transfer between the fuel and cladding (including conductance, radiation, and contact pressure terms), heat transfer to the coolant, and other phenomena. Details are given in (Williamson et al., 2012). Primary differences between BISON and traditional nuclear fuel performance codes include BISON's ability to solve problems on a general, user-defined mesh, and the fact that BISON may run in parallel to solve large problems.

To solve coupled systems of physics equations, BISON utilizes the Jacobian-free Newton Krylov (JFNK) method (Knoll and Keyes, 2004). JFNK is particularly useful in a multiphysics setting. This is due to the fact that the JFNK technique does not require the exact Jacobian. Only the residual contributions of the primary variables are needed. In a complex multiphysics problem, where variables are coupled to one another in complex ways, the ability to solve the analysis without the need to derive, code, and debug the exact Jacobian provides a distinct benefit.

2.1. Static Equilibrium

Momentum conservation is prescribed assuming static equilibrium at each time increment using Cauchy's equation,

$$\nabla \cdot \boldsymbol{\sigma} + \rho \mathbf{f} = 0, \tag{1}$$

where $\boldsymbol{\sigma}$ is the Cauchy stress tensor and $\mathbf{f}$ is the body force per unit mass (e.g. gravity). Constitutive relations are used to calculate the stress from the strain, which is in turn related to the displacement vector $\mathbf{u}$ through kinematic relations.

For the case of linear elasticity,

$$\boldsymbol{\sigma} = \boldsymbol{C}[\boldsymbol{\varepsilon} - \boldsymbol{\varepsilon}_T] \tag{2}$$

where $\boldsymbol{C}$ is the fourth-order elasticity tensor, $\boldsymbol{\varepsilon}$ is the total strain, and $\boldsymbol{\varepsilon}_T = \alpha(T - T_0)\boldsymbol{I}$ is the thermal strain with T as temperature, T_0 as original temperature, and $\boldsymbol{I}$ as the identity tensor. Static equilibrium therefore depends on the thermal solution.

2.2. Heat Conduction

The heat conduction equation is

$$\rho C_p \frac{\partial T}{\partial t} - \nabla \cdot (k \nabla T) - q = 0, \tag{3}$$

where T, ρ and C_p are the temperature, density and specific heat, respectively, k is the thermal conductivity of the material, and q is a volumetric heat generation rate.

2.3. Gap Heat Transfer

When analyzing heat transfer between independent bodies, heat conduction across a gap must be addressed. In this work, gap conductance h in a gas-filled gap between two surfaces is described using the form proposed in (Ross and Stoute, 1962):

$$h = \frac{k_g(T_g)}{L_g + C_r(r_1 + r_2)} \tag{4}$$

where k_g is the thermal conductivity of the gap medium, T_g is the temperature in the gap, L_g is the gap length, and r_i is a distance associated with the roughness of the i side of the gap. Gap heat conduction therefore depends on the static equilibrium solution through the gap length. The nonlinear dependence of h on the gap length is shown in Figure 1.

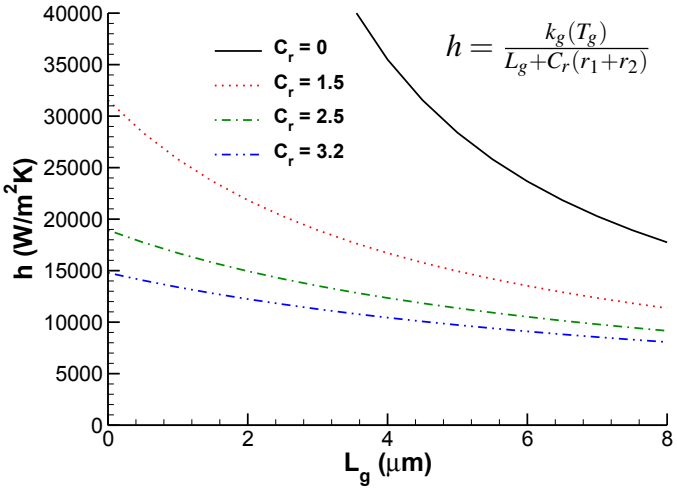

Figure 1: Gap conductance h as a function of gap length L_g with different roughness coefficients for $k_g = 0.142$ W/m/K, $r_1 = 1 \times 10^{-6}$ m, and $r_2 = 2 \times 10^{-6}$ m.

2.4. Jacobian-free Newton Krylov

To solve a nonlinear system of equations, it is common to begin with a residual statement (Hales et al., 2012)

$$\mathbf{r}(\mathbf{x}) = 0 \tag{5}$$

where $\mathbf{r}$ is the residual with $\mathbf{x}$ as the unknown solution. The Jacobian is written as

$$\mathbf{J}(\mathbf{x}) = \frac{\partial \mathbf{r}(\mathbf{x})}{\partial \mathbf{x}}. \tag{6}$$

Newton's method is then

$$\text{Compute } \mathbf{J}(\mathbf{x}_k), \mathbf{r}(\mathbf{x}_k) \tag{7}$$

$$\text{Solve } \mathbf{J}(\mathbf{x}_k)\mathbf{s} = -\mathbf{r}(\mathbf{x}_k) \text{ for } \mathbf{s} \tag{8}$$

$$\mathbf{x}_{k+1} = \mathbf{x}_k + \mathbf{s} \tag{9}$$

which is continued until the update is sufficiently small or some other criterion is met.

The JFNK method evaluates the action of the Jacobian through a finite difference approximation,

$$\mathbf{J}(\mathbf{x}_k)\mathbf{v} \approx \frac{\mathbf{r}(\mathbf{x}_k + \varepsilon \mathbf{v}) - \mathbf{r}(\mathbf{x}_k)}{\varepsilon}. \tag{10}$$

This is an attractive form since neither the full Jacobian nor its element-by-element contributions are required. Despite not requiring the analytic Jacobian, the effect of the full Jacobian is seen from the first iteration of the iterative solver, unlike modified Newton or quasi-Newton algorithms. Thus, with only GMRES (Saad and Schultz, 1986) (which does not require $\mathbf{J}$ but $\mathbf{Jv}$) and a function that computes the residual, JFNK finds solutions to nonlinear coupled equations with the convergence rate of a traditional Newton algorithm.

JFNK, like Newton's method, is a general technique for solving nonlinear equations. As such, it provides BISON with flexibility in selecting which phenomena are active in a given simulation as well as flexibility in choosing which model to activate for a given phenomena. This generality is due to the fact that the approach is based on the evaluation of the residual, which is done according to whatever models and options are active for a given analysis.

Efficient solves using iterative methods require good preconditioners. The purpose of preconditioning is to decrease the condition number of the system being solved. Equivalently, preconditioning reduces the spread of eigenvalues in the system. In JFNK, it is common to use right preconditioning,

$$\mathbf{J}(\mathbf{x}_k)\mathbf{M}^{-1}(\mathbf{M}\,\mathbf{s}) = -\mathbf{f}(\mathbf{x}_k) \tag{11}$$

where $\mathbf{M}$ is the preconditioner or preconditioning process. In this form, the solution approach involves two steps. First, solve $\mathbf{J}(\mathbf{x}_k)\mathbf{M}^{-1}\mathbf{w} = -\mathbf{f}(\mathbf{x}_k)$ for $\mathbf{w}$. Then, compute $\mathbf{s} = \mathbf{M}^{-1}\mathbf{w}$. Note that if $\mathbf{M}^{-1} = \mathbf{J}^{-1}$ the iterative solve will converge in one iteration. However, computing $\mathbf{J}^{-1}$ is equivalent to solving the original system and so is not advantageous. It is necessary, therefore, to choose a preconditioner that reflects the character of $\mathbf{J}(\mathbf{x}_k)$ in order to accelerate the iterative method but also one that is inexpensive to compute and apply. Simple approximations to sub-blocks of the Jacobian along the diagonal may suffice.

BISON commonly uses an algebraic multigrid preconditioner, while other preconditioners are available (Hales et al., 2012).

3. Coupling Strategies

The strategies used to solve coupled sets of physics equations can be generally categorized as loose coupling and tight coupling. In loose coupling, the distinct physics in a coupled problem are solved individually, keeping the solutions for the other physics fixed. After a solution is obtained for an individual physics, it is transferred to other physics that depend on it, and solutions are obtained for those physics.

These fixed-point, or Picard, iterations are repeated until convergence is obtained. If there is not a strong two-way feedback between the physics involved, convergence can be obtained quickly with a minimal number of loose-coupling iterations. An advantage of this approach is that it allows for independent codes to be coupled with relatively minor modifications to those codes, and they can each use their own solution strategies that are tailored for their solution domain. The disadvantage of loose coupling is that if there is strong two-way feedback between the physics, the approach can have an unacceptably slow convergence rate and is more likely to encounter convergence difficulty (Novascone et al., 2013).

In tight coupling solution methods, a single system of equations is assembled and solved for the full set of coupled physics. The nonlinear iterations operate on the full system of equations simultaneously, taking into account the interactions between the equations for the coupled physics in each iteration. In cases where there is strong coupling between the physics, this approach can have faster convergence rates than loose coupling.

The primary disadvantage of this approach is that it necessitates tighter coordination between the codes to solve the individual physics.

For thermomechanical problems, in the absence of evolving contact between components, the coupling between the heat conduction and solid mechanics equations is often primarily one-way. The temperatures obtained from the heat conduction equations cause thermal strains, which result in displacement of the mechanical model. These displacements typically have a negligible effect on the thermal model, and such problems can be readily and accurately solved using loose coupling strategies, or even by transferring data from a thermal code to a solid mechanics code and completely neglecting the effect of the mechanical solution on the thermal solution.

Introducing evolving mechanical and thermal contact to thermomechanical problems transforms them from being essentially one-way coupled problems to strongly two-way coupled problems. This is because the conductance across gaps between adjacent bodies is highly dependent on the distance between those bodies, which is a function of the solid mechanics solution. Because the fuel system used in LWRs relies on heat transfer across the evolving fuel/cladding gap, the ability to solve the strongly coupled thermal and mechanical equations in the presence of evolving contact conditions is critical for a successful fuel performance modeling code.

As mentioned previously, BISON by default solves this full set of equations (Equations 1 and 3) in a tightly coupled manner using the JFNK solution method. It is also possible to run BISON in a loosely coupled mode in which a series of fixed-point, loose coupling iterations are taken to solve the full set of coupled equations. This facilitates a comparison of the two solution strategies. When run in a loose-coupling mode, in each loose coupling iteration, BISON first uses JFNK to solve the thermal equations, keeping the solid mechanics solution fixed. BISON then uses JFNK to solve the solid mechanics equations, keeping the thermal solution fixed. For the solutions of these individual physics problems, nonlinear iterations are repeated until the convergence tolerance is reached. The loose coupling iterations are repeated until the residuals are below the loose coupling convergence tolerance (until the solution in each physics is no longer changing).

The same nonlinear tolerance was used for both the loose and tight coupling cases. As long as the tolerances are sufficiently tight (small), the results from the two approaches are effectively the same. The same thermal, mechanical, fission gas, etc. models may be used with either coupling approach.

Tightly and loosely coupled strategies were evaluated using a 2D axisymmetric simulation of a short section of a LWR fuel pin. The assumed geometry, shown in Figure 2, includes ten individual UO_2 pellets, Zr-4 cladding, an initial 80 μm pellet-clad gap, and an open region to simulate the upper plenum. A uniform convective boundary at the clad outer wall simulates heat transfer to the flowing coolant. Typical PWR operating conditions were used, as given in Table 1. The rod power was assumed to rise linearly over three hours and held constant for 3.2 years. An axial power profile was applied to the fuel to demonstrate this capability, which would be applicable for a full-length rod. A typical finite element mesh consisting of linear quadrilateral elements is also shown in Figure 2. The finite element mesh for this study has 18710 elements (7 elements through the clad thickness, 22 elements radially and 64 elements axially for each pellet).

Table 1: Simulation input parameters for the 2D axisymmetric model used to investigate tight and loose coupling strategies.

Linear average power (W/cm)	200
Fast neutron flux (n/m^2/s)	9.5×10^{17}
Coolant pressure (MPa)	15.5
Uniform coolant temperature (K)	530
Coolant convection coefficient (W/m^2/K)	7500
Rod fill gas	Helium
Fill gas initial pressure (MPa)	2.0
Initial fuel density	95% theoretical

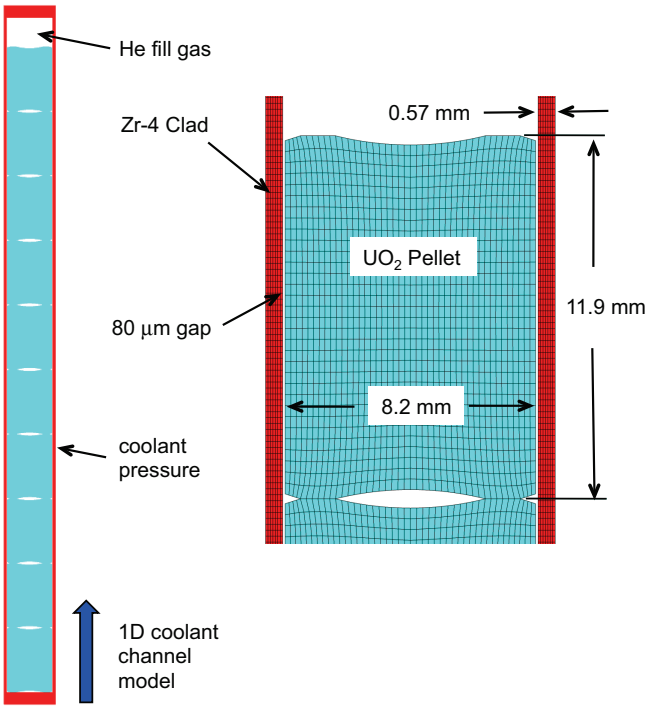

Figure 2: Fuel pin model description of geometry, materials, mesh, and boundary conditions.

The thermal conductivity of the fuel was simulated using the temperature and burnup dependent Fink-Lucuta approach (Fink, 2000; Lucuta et al., 1996). The Young's modulus, Poisson's ratio, and thermal expansion coefficient for the fuel were assumed constant at 219 GPa, 0.345, and 10×10^{-6} 1/K respectively, as given by Olander (Olander, 1976). The thermal conductivity, Young's modulus, Poisson's ratio, and thermal expansion coefficient of Zr-4 were assumed constant at 16 W/m/K, 75 GPa, 0.3, and 5.0×10^{-6} 1/K respectively, using typical values from MATPRO (Allison et al., 1993). Mechanical contact between the fuel and clad was assumed to be frictionless.

Much more detailed information regarding the material models used and detailed results of this problem can be found in (Williamson et al., 2012). The main emphasis here is to compare the effectiveness of the tight and loose coupling strategies.

Plots of iteration counts to solve each time step, generated to assess the difference in computation costs between the tightly and loosely coupled approaches, are shown in Figure 3. This plot shows the number of nonlinear iterations to solve the thermomechanical equations as a single tightly coupled system for each step. In addition, for the loosely coupled solution strategy, it shows the number of loose-coupling (fixed-point) iterations, the average number of nonlinear iterations per loose-coupling iteration, and the total number of nonlinear iterations for each step. The total number of nonlinear iterations is much higher for the loosely coupled case than for the tightly coupled case, and there is corresponding increase in solution time required for the loosely coupled case. The tightly and loosely coupled cases ran in about 3 and 5 hours, respectively, on a workstation using 8 processors. The memory requirements for the cases were similar.

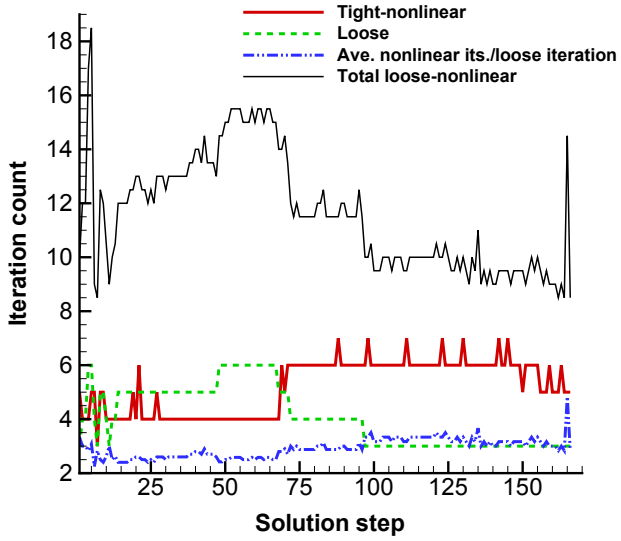

Figure 3: Iteration count for tight and loose coupling strategies during the single fuel pin simulation.

There are a few interesting points to note regarding the iteration counts in Figure 3. One is that the fuel-clad gap closes (at the center of the fuel column) at time step number 68. This corresponds to an increase in the number of tightly-coupled nonlinear iterations and a decrease in the number of loosely-coupled nonlinear iterations. This behavior is somewhat unexpected but may be due to the interaction of mechanical and thermal contact along with how differences in those models respond with tight and loose coupling strategies. This will be further investigated in the future.

Also notable is the sharp increase in the number of loosely coupled nonlinear iterations at the end of the simulation. This is likely due to the rapidly increasing fission gas release at this point in the simulation. The loosely coupled approach is known to have more difficulty in achieving convergence as the gap is closing and the thermal conductivity in the gap is decreasing due to increasing fission gas release (Novascone et al., 2013). This was evident when an attempt was made to further tighten the tolerances. The tightly coupled approach successfully obtained a converged solution, while the loosely coupled approach did not.

In general, problems that involve two-way coupled equations (such as nuclear fuel analysis with a small gap) benefit from using a tight coupling strategy. This combination of tight coupling and JFNK provides a flexible and robust solution approach. This approach accommodates developing new mechanical models, thermal models, or other behavioral models without the need to adjust the overall solution methodology.

4. Neutronics Coupling

Another example of multiphysics coupling for LWR analysis is that of neutronics and thermomechanics. A number of different strategies for coupling have been performed in the past (Lee et al., 2000; Lemehov et al., 2001; Hamilton et al., 2012; Hursin et al., 2013; Soba et al., 2013) with different types of data transfer and levels of fidelity. This paper demonstrates coupling of a high-fidelity core analysis program, DeCART (Joo et al., 2004), to BISON. DeCART provides BISON with a sub-pin level resolution of the pin power density, fission rate density, and the fast flux (for a specified energy cut-off) during depletion or a fast transient simulation. The temperature distribution, in turn, is mapped from BISON back to DeCART, resulting in full two-way coupling. A Picard iterative algorithm is used to converge the two physics, similar to the loose-coupling strategy described above. Simulation results given here focus on the error associated with the mapping of data, and a well known high burn-up model is used for comparison (Lassmann et al., 1994). Conditions are applied and modeled where this model is known to be valid.

4.1. Overview of DeCART

For nuclear reactor simulations, the equations for the radiation field density and isotopic composition are solved to obtain the different reaction rates, which include the fission reaction for calculation of the power density and the critical eigenvalue or k_{eff}, which is a measure of the ratio of neutron production to loss. A differential balance of the radiation field over a small volume results in a neutron density equation called the Boltzmann transport equation, and a detailed description of its derivation can be found in the literature (Lewis and Miller, 1984). DeCART solves the three-dimensional neutron transport equation with the 2-D/1-D method (Joo et al., 2004; Kelly and Larsen, 2013; Kelly et al., 2013) where each radial plane is solved by the Method of Characteristics (MOC) and the axial direction is resolved with a Nodal Expansion Method. To evaluate the Boltzmann neutron transport equation, the material neutronic properties given by neutron cross sections must be specified or calculated. Cross sections are affected by the material temperature, which broadens the cross section resonance

structure. DeCART applies a sub-group resonance treatment to help calculate the cross sections for a specified temperature distribution (Joo et al., 2004).

In addition, fissionable isotopes are consumed by the fission reaction, and other isotopes are transmuted by neutron capture. The neutron cross sections change over time as this isotopic content of the fuel changes. This change is calculated by numerically solving the depletion equations (Gould et al., 2009) using the matrix exponential method (Gould et al., 2009) where sub-steps are used if needed. For sub-step calculations, the one-group cross sections are updated by the depletion calculation, but the scalar flux is not.

4.2. Coupling Method

The finite element meshes for BISON and finite volume regions for DeCART are not expected to match, nor are they expected to coincide in any way. This is due both to the use of different numerical solution techniques and the need to resolve different physics within the two codes. This section briefly describes the data representation on each mesh and the technique used to map the data from the source mesh to the target mesh.

DeCART models a fuel pin with a structured mesh, dividing the pin into equal sub-volume regions in the radial direction which are referred to as DeCART regions. The fission rate and power density are represented as volumetric averages over individual DeCART regions, with the average fission rate and power densities calculated by integrating the product of the fission cross section and scalar flux over the entire energy range and the volume associated with a specified node in its mesh. The term is divided by the total volume of the specified region to obtain the volumetric average. The neutronics calculation requires a fine mesh on the outer radial rod boundary to capture the neutron induced rim effect (Lassmann et al., 1994) but allows for a coarser mesh in the fuel center where the profile is relatively flat.

BISON is finite element based and solves the fuel pin thermomechanics on an unstructured mesh. In BISON, the fission rate density and power density may be represented either as interpolations from values defined at the finite element nodes or as values that are uniform within each element. The elements in the unstructured BISON mesh are often evenly distributed radially to capture phenomena of interest to fuel performance analysis.

To transfer data between the mismatched meshes, the fission rate density and power density at each BISON mesh node are set to the average volumetric fission rate and power density in the DeCART region in which they are located, as illustrated in Figure 4. This type of mapping allows the basic fission rate and power density shape to be preserved but does not preserve the total rod power. The DeCART fission and power density rate at each time step are mapped to the corresponding original undeformed finite element node locations in BISON. No extrapolation is applied to the DeCART power or fission rate density for the values at the fuel rim. The BISON nodes are allowed to move, but obtain their values at each timestep from the undeformed mesh state. The DeCART mesh does not deform.

After transferring the data, the fission rate and power density in BISON are scaled to preserve the total rod power. The preservation factor is given by

$$f(t) = \frac{P_{DeCART}}{P_{BISON}} \tag{12}$$

and is the ratio of the total power calculated by DeCART to the total power calculated by BISON. At each BISON time step, the fission rate density points are multiplied by the preservation factor so that the net total power from DeCART is preserved.

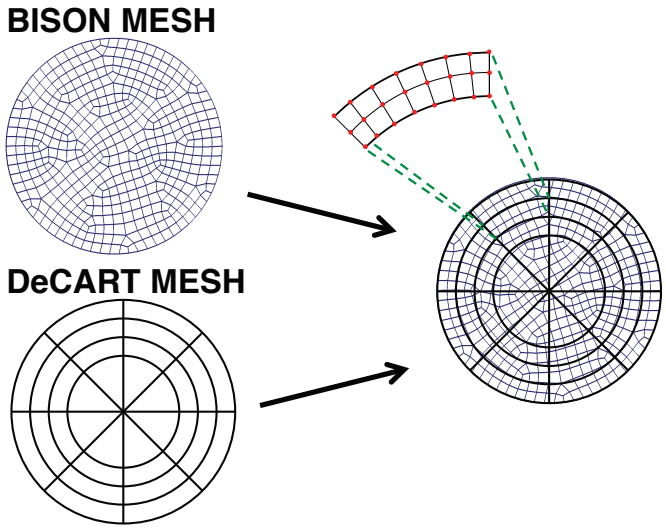

Figure 4: Illustration of the simple mapping scheme for data transfer from DeCART mesh to BISON mesh. All BISON nodes (points) residing in a DeCART node (volumes) receive identical data.

DeCART and BISON were compiled into a single application that allows memory-based data transfers between the two codes. Interfaces were created to allow function calls to obtain the total rod power and power and fission rate densities for a given time directly from DeCART. The DeCART depletion routines run at user specified time steps through the internal time marching algorithm in BISON.

The algorithm for two-way coupling works as follows: first, both the DeCART and BISON input files are read, and the codes are initialized. A steady state DeCART calculation is executed, and the fission rate density and power density are saved. Next, BISON takes a time step and solves the thermomechanics equations with the JFNK solver using the saved DeCART fission rate density and power density data. A DeCART depletion step is then performed, temperatures from the current BISON calculation are mapped to the DeCART mesh, and the neutron cross sections are updated. An iteration loop is then entered where DeCART and BISON are solved in steady state with temperatures and fission rate densities transferred between the two. As mentioned above, this loop is sometimes referred to as a Picard or function iteration. After performing a specified number of iterations or meeting a pin eigenvalue convergence criteria, DeCART takes another depletion time step. This scheme continues until the specified end time is reached.

To calculate an average region temperature for DeCART, a volume average temperature is computed over all BISON elements coincident with the DeCART regions of fuel and cladding. The original undeformed BISON mesh is used in determining which elements to include in the volume region average. The temperature at the cladding boundary is specified for BISON, and the bulk water temperature is specified for the DeCART neutronics. Consistent water temperature and effects will be addressed in the future.

4.3. Results with One-way Coupling

A study of the radial mesh density for DeCART and BISON was performed and is important since the number of DeCART radial regions and the number of radial elements in BISON determines how well the neutronic rim effect is captured and mapped. For this set of results, the radial mesh is refined more than is typical in an assembly or core calculation. The neutronic rim effect is explicitly resolved and the power and fission density rates are refined to be internally smooth to avoid potential effects from artificial stepping (Hamilton and Clarno, 2011). The results shown in this study were obtained from a simulation with one-way data transfer from DeCART to BISON. Thus, the temperatures for the DeCART calculation are prescribed for the fuel, cladding, and water regions.

The DeCART model is a single box fuel pin lattice or a square domain with coolant surrounding the pin. For DeCART, the fuel pin consists of the cladding, gap and the central fuel pellet region. Reflective boundary conditions were specified on the lattice top and bottom and on all sides of the coolant channel. Thus, the DeCART model shows variations in the radial direction only. The BISON domain includes only the fuel pellet and cladding. A list of properties used by each application is given in Table 2.

Table 2: Fuel rod properties for one- and two-way coupling of DeCART and BISON.

Rod Height (m)	3.66
Fuel Pellet Radius (m)	0.0041
Gap Width (m)	8.0e-05
Cladding Width (m)	5.7e-04
UO_2 weight percent	4
Cladding Material	ZR2
DeCART Cladding Temperature (K)	580
DeCART Fuel Temperature (K)	847
BISON Cladding Temperature (K)	580
Linear Power Rate (kW/m)	18.9

Figures 5 and 6 show the developed fission rate density and temperature after one year of depletion. In Figure 5, fission density rates for different DeCART radial fuel divisions are mapped to a fixed BISON QUAD-4 mesh with eleven radial element subdivisions in the fuel, and the calculated temperatures from the fission rate densities are shown in Figure 6. The fission rate density is normalized to give the total rod power calculated by DeCART. BISON results using the internal Lassmann radial pow
both

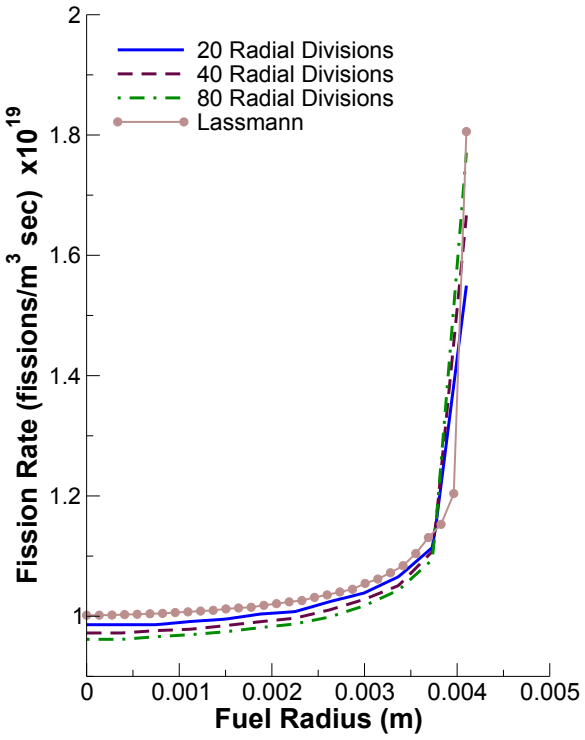

Figure 5: Fission rate densities at one year of depletion generated by DeCART and mapped to a fixed BISON QUAD-4 mesh. The number of DeCART radial subdivisions in the fuel are listed in the caption.

In Figure 6, higher fuel pin center temperatures correspond to higher fission rate densities across the center of the fuel. Figure 5 shows that a higher fission rate density at the fuel rod edge is obtained for an increasing number of DeCART mesh volumes. The higher fission rate density at the fuel rod edge results in a higher total power when mapped to the BISON mesh and is scaled to preserve the total rod power calculated by DeCART. This scaling results in a lower fission rate density across most of the fuel pin and a lower temperature across the fuel pin. Thus, Figures 5 and 6 show a decreasing temperature and fission rate density profile for an increasing number of DeCART radial subdivisions on the fixed QUAD-4 BISON mesh. To capture the detail provided by the DeCART flat source mesh, the BISON finite element QUAD-4 mesh must be at least as fine in the region around the rim.

Effects of varying the BISON radial mesh density are shown in Figures 7 and 8. Here the fission rate density was generated with forty DeCART radial mesh divisions and mapped onto different BISON meshes composed of either linear (QUAD-4) or quadratic (QUAD-8) elements. The computed fission rate profile falls below the Lassmann prediction when only ten linear elements are provided. Twenty or forty linear elements give a result much closer to the Lassmann result. Note that ten quadratic elements capture the steep fission rate density profile nicely. Figure 7 shows that the linear elements can accurately capture the steep fission rate profile if there are a sufficient number of

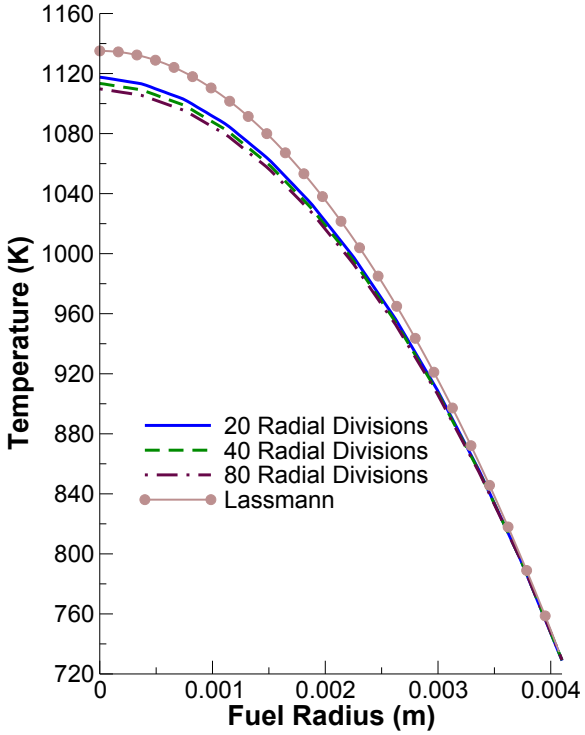

Figure 6: Temperature distributions at one year of depletion for a fixed BISON QUAD-4 mesh. The number of DeCART radial subdivisions in the fuel are listed in the caption.

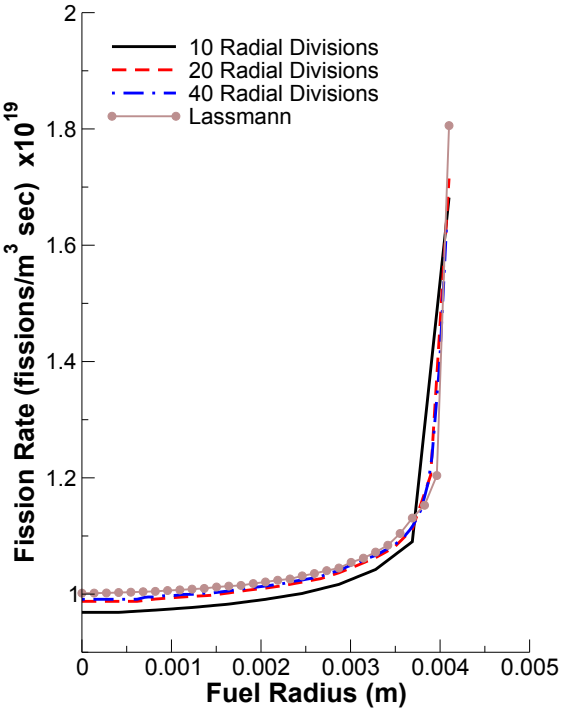

Figure 7: The fission rate density at one year of depletion generated by DeCART and mapped to a different BISON QUAD-4 mesh. The number of radial subdivisions in the fuel for the BISON mesh are listed in the caption.

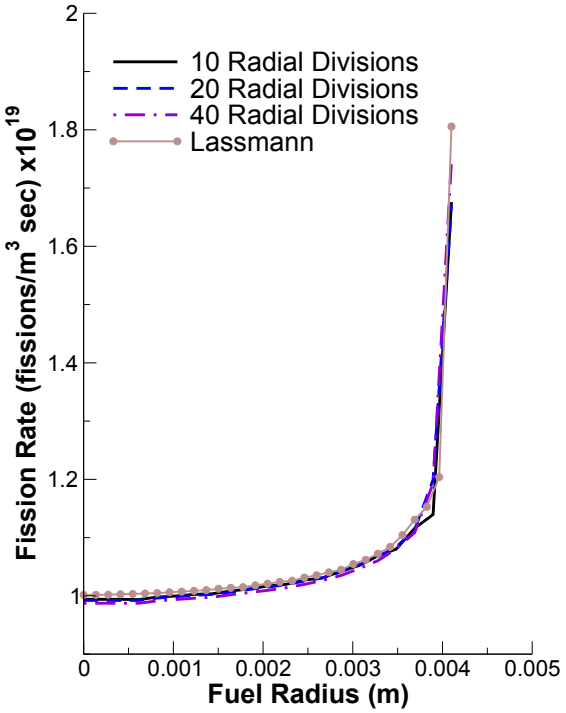

Figure 8: The fission rate density at one year of depletion generated by DeCART and mapped to a different BISON QUAD-8 mesh. The number of radial elements in the fuel for the BISON mesh are listed in the caption.

elements to roughly resolve the fission rate profile generated by DeCART. Figure 8 shows that fewer quadratic elements are needed because they are able to locally capture the smooth and steep fission profile.

4.4. Results with Two-way Coupling

For a single fuel pin, a two-way coupled analysis was also performed. In this case both the DeCART and BISON domains are axisymmetric; thus, the BISON domain is modeled using a 2D RZ mesh. For the fuel cell in DeCART, zero incoming currents are prescribed at the top and bottom, and reflective boundaries are set on the four edges of the water channel, making the DeCART fuel pin an infinite lattice. The details of this fuel pin are in Table 2. The temperature is specified on the outer cladding surface in BISON. Fission rate density calculated by DeCART was mapped to BISON while temperature computed by BISON was mapped back to DeCART. A Picard iteration was performed on the temperatures and fission rate density, using the two-way coupling algorithm outlined above. Iterations were fixed at four per time step.

Data are given in Table 3 for each iteration during the final time step of the simulation. The table shows the last calculated pin eigenvalue (k_{eff}), the relative error in k_{eff} in per cent mille (pcm), and the L^2 and L^{inf} norms of the relative error in the fission rate density on the DeCART mesh. As shown in Table 3, k_{eff} shows rapid convergence at the final time step,and both norms show rapid convergence for the fission rate density. This rapid convergence was present in all time steps, and additional

simulations were performed with the two-way data transfer that also demonstrated rapid convergence.

The centerline temperatures were compared for the internal BISON Lassmann style model, the one-way coupled DeCART and BISON approach, and the two-way coupled DeCART and BISON approach. Expected agreement is obtained for an appropriately meshed Lassmann style model and the one-way coupled DeCART and BISON model.

However, the two-way coupled DeCART and BISON model produces results that are cooler than either the one-way or the internal Lassmann model. A higher peak for the rim power density rate and larger self shielding is observed when pin temperatures are applied in DeCART. This lowers the power density rate at the pin center and thus lowers the pin centerline temperature. These results suggest that a two-way coupling scheme between BISON and DeCART is both feasible and stable; however, further investigation is needed to establish overall accuracy and quality of the coupling scheme. These studies should include examination of the effect of different radiation-induced thermomechanics-related physics (such as radiation induced creep and fission gas swelling) on the coupling scheme, the effect of different convergence criteria, and the accuracy with different mesh densities for both codes.

For both one-way and two-way coupling, the additional expense of performing neutronics calculations may seem unnecessary since coupling does not produce a higher fidelity solution when compared to current internal models for simple pin cell problems. However, simple pin cell problems help establish the fidelity of the data transfers. These data transfers must be of sufficient accuracy to produce meaningful results for more complex scenarios to be studied in the future.

5. Multiscale Coupling

As a final example, the need for multiscale coupling is considered. Throughout its lifetime in a reactor, the fuel undergoes significant microstructure evolution due to elevated temperature, stress, and radiation damage. These microstructural changes directly impact the fuel performance, degrading the material properties. For example, fission gas production and evolution causes swelling, a reduction in the thermal conductivity, and fission gas release. The mechanisms involved in the microstructure evolution occur at the atomistic and grain scale and are therefore below the resolution of a fuel performance code. Traditionally, these effects are considered using empirical or semi-empirical material models. These models are typically fit to experimental data for LWRs and correlated to burnup and temperature. While these models can accurately interpolate within testing limits, they cannot accurately extrapolate outside these limits to analyze new concepts or accident conditions. However, it is possible to use lower lengthscale models, such as INL's MARMOT code, to predict microstructure evolution and how it impacts bulk material properties, such as swelling or thermal conductivity. Thus atomistic and mesoscale modeling and simulation is coupled to the fuel performance code to provide a multiscale modeling capability.

There are two main approaches for multiscale coupling: hierarchical and concurrent. In hierarchical coupling, lower lengthscale simulations are conducted separately, to explore the material response within the space defining all possible conditions. The best results occur when the lower lengthscale data is used to inform and verify a mechanistic material model that can be directly implemented in the fuel performance code. In concurrent coupling, the fuel performance code and the lower lengthscale simulations are run concurrently, with information being passed between the scales. Concurrent coupling provides a superior description of the multiscale behavior, as the interactions between the scales are fully resolved, but it can be very computationally expensive. Thus, hierarchical coupling is used to provide lower lengthscale input to production codes, while concurrent coupling can be used to investigate the multiscale interactions in great detail and refine the hierarchical models, when necessary.

BISON has been used in both hierarchical and concurrent coupling using the MARMOT code. Here, the MARMOT code is summarized and both concurrent and hierarchical multiscale coupling are demonstrated.

5.1. Overview of MARMOT

MARMOT is a multiphysics mesoscale code that predicts the co-evolution of microstructure and properties due to applied load, temperature and radiation damage (Tonks et al., 2012). MARMOT employs the phase field (PF) model to predict the microstructure evolution, coupled with finite deformation solid mechanics and heat conduction. The PF model is a powerful tool for modeling microstructure evolution under irradiation (Hu et al., 2009; Hu and Henager Jr, 2009; Millett et al., 2011a,b; Millett and M., 2010), and for this reason MARMOT uses the PF method tightly coupled with finite deformation mechanics and heat conduction and solved with FEM using the MOOSE framework. MARMOT has been used to model void and bubble nucleation, growth and migration (Tonks et al., 2012; Zhang et al., 2012a), phase separation (Zhang et al., 2012b), grain boundary (GB) migration and grain growth (Tonks et al., 2013b, 2014) and crystal plasticity (Chockalingam et al., 2012b). It has also been used to determine the impact of microstructure on properties, such as the thermal conductivity (Tonks et al., 2013a; Millett et al., 2013). Though MARMOT is a mesoscale code, atomistic density functional theory and molecular dynamics (MD) simulations are used to investigate basic mechanisms and provide necessary atomistically-informed parameter values (Tonks et al., 2013b,a). In addition, new models can be rapidly developed within MARMOT.

5.2. Concurrent Coupling

By concurrently coupling MARMOT to BISON, radiation induced microstructure evolution is directly accounted for, as is the interaction between the meso- and macroscales. The first simulations to ever concurrently couple mesoscale simulations with a macroscale fuel performance code were performed using a phase field model with the BISON code (Tonks et al.,

Table 3: Picard iteration convergence data for single fuel element at final time step.

Iteration	k_{eff}	Relative Error in k_{eff} (pcm)	L^2 Norm of Relative Error in Fission Rate Density	L^{inf} Norm of Relative Error in Fission Rate Density
1	1.168018	-	-	-
2	1.168018	4.430×10^{-5}	4.647×10^{-10}	1.611×10^{-9}
3	1.168018	9.505×10^{-11}	1.535×10^{-13}	3.631×10^{-13}
4	1.168018	3.802×10^{-11}	9.111×10^{-15}	2.268×10^{-14}

2010). Since then, BISON has also been concurrently coupled to MARMOT, with mesoscale simulations placed at positions of interest within the macroscale model (Williamson et al., 2012). This capability is demonstrated by summarizing this calculation from Williamson et al. (2012). Full details on the calculation will not be given here but can be found in the original paper.

Here, transient phase field MARMOT simulations are coupled to a transient, multiphysics BISON simulation. This is a proof-of-concept simulation and does not represent an accurate description of the multiscale physics. The BISON simulation is a 2D axisymmetric model of a five pellet rodlet similar to the ten pellet rodlet shown in Figure 2. The material models are identical to those used above except for the thermal conductivity, which is taken from the mesoscale simulations. Four simulations of bubble nucleation and growth in a micron square of UO_2 are solved using the void growth model from (Tonks et al., 2012) in which only the vacancy concentration is considered. Both interstitials and gas atoms are neglected in this simple model. Note that due to the simplicity of this model, bubble nucleation occurs much later than the true physical behavior. A random source term accounts for vacancies generated due to radiation and is a function of the neutron flux. A steady-state heat conduction calculation is coupled to the phase field model to determine changes in the bulk thermal conductivity (Tonks et al., 2012), where the voids are given the local thermal conductivity of Xe gas and the bulk is given the thermal conductivity of unirradiated UO_2 at the temperature provided by the BISON simulation (Fink, 2000). The temperature is calculated across the domain by solving Eq. (3), with a constant temperature applied to the left side of the simulation and a fixed heat flux applied to the right. The full details for this calculation are given in Williamson et al. (2012).

The BISON simulation is loosely coupled to the four MARMOT simulations, with the BISON calculation occurring first at each time step. The mesoscale simulations are assigned to the center of the middle pellet, the outer edge of the middle pellet, the center of the bottom pellet and the edge of the bottom pellet, and the corresponding temperature and neutron flux are passed down to define the conditions of the corresponding phase field simulations. The four microstructures are evolved and the thermal conductivity is calculated at the four positions. These values are then linearly interpolated throughout the five pellets, with the thermal conductivity of the bottom pellet mirrored to the top pellet. The interpolated values are used in the BISON simulation at the next time step. All the simulations take the same time step, following the smallest required time step of the five simulations. Note that to accurately calculate the void behavior across the pellet radius would require many more divisions than just the two employed here.

The temperature profile in the rodlet after three years is shown in Figure 9(a) and the final microstructure at the four locations within the rodlet are shown in Figure 9(b). The bubbles are largest at the center of the middle pellet, due to the high temperature and neutron flux. At the outer edge of both pellets, the temperature is too low for significant vacancy diffusion and clustering. Thus, no bubbles form. Before the formation of the bubbles, the time step was quite high ($\sim$ 50 days) as shown in Figure 9(c). However, once bubbles begin to nucleate, the time step dropped three orders of magnitude to 0.01 days.

The thermal conductivity experiences initial changes due to changes in the fuel temperature (as the temperature goes down, the thermal conductivity goes up and vice versa, as shown in Figures 9(d) and 9(e)). However, once the pores nucleate and grow in the hotter center region after two years in the reactor, the thermal conductivity rapidly decreases at the center. Due to this drop, the temperature rises throughout the rodlet (Figure 9(e)), accelerating the nucleation in the center of the bottom pellet. Thus, the interaction between the scales plays an important role in bubble nucleation and thus thermal conductivity behavior. However, this high fidelity interaction comes at a large computational expense. In this case, the size of each of the four mesoscale MARMOT simulations is on the same order as the macroscale BISON, such that the concurrently coupled simulation is five times more computationally expensive than a similar uncoupled BISON calculation.

5.3. Hierarchical Coupling

In hierarchical coupling, lower lengthscale simulations are conducted beforehand, and are used to inform the development of an analytical model that accounts for the lower lengthscale physics. This approach is demonstrated here by taking an example from (Tonks et al., 2013a) in which a model is developed that captures the impact of GB fission gas bubbles on the UO_2 fuel thermal conductivity. The model is summarized here but is given in more detail in (Tonks et al., 2013a).

The fission gas that develops within the fuel degrades the fuel thermal conductivity, contributes to fuel swelling, and results in fission gas release. However, in typical fuel performance codes, the thermal conductivity model is independent of the fission gas behavior. In two-stage fission gas release models (Dowling et al., 1982; Forsberg and Massih, 1985), the fission gas is assumed to be uniformly produced within the grain and then to diffuse to the GB. Once the fission gas on the GB reaches a

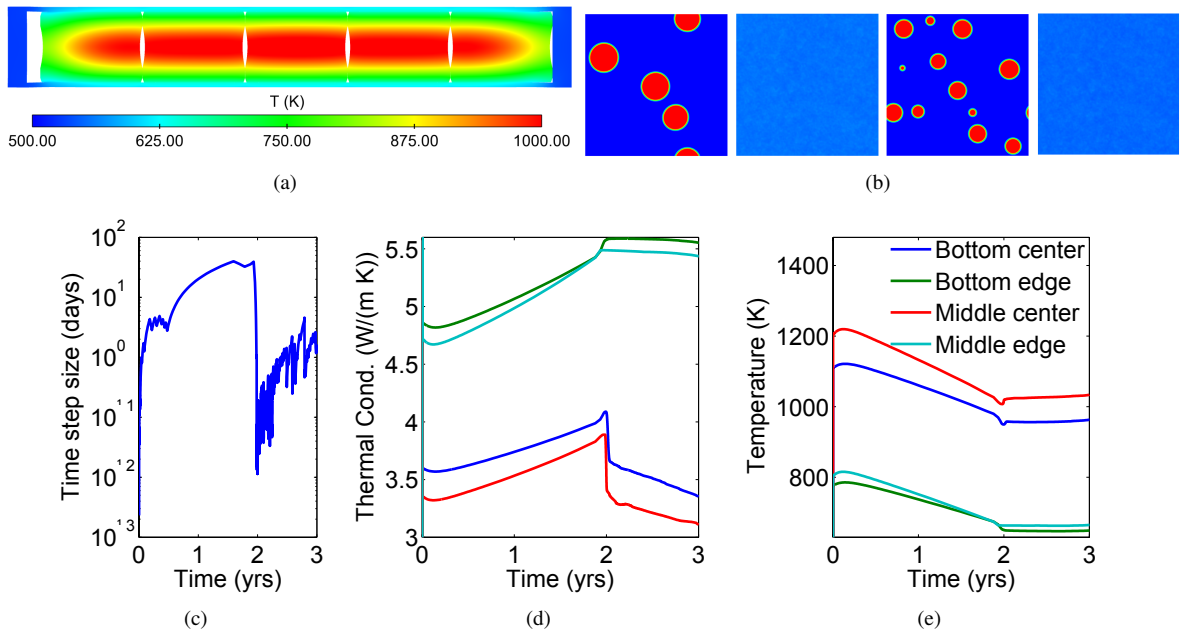

Figure 9: Multiscale simulation results, where (a) shows the final geometry of the rodlet and (b) shows the final microstructure at the center of the middle pellet (left), outer edge of the middle pellet (left center), center of the bottom pellet (right center) and the edge of the bottom pellet (right). In addition, the behavior of the time step during the simulation is shown in (c), and the thermal conductivity (d) and temperature (e) are shown vs time at the four locations (from (Williamson et al., 2012)).

critical percolation threshold, it begins to be released into the gap. Hence, at any point in time, some fission gas is located in the grain interior and some is concentrated on the GB. This work uses the semi-empirical model from (Forsberg and Massih, 1985). However, in the future more physics-based models, like that from (Pastore et al., 2013), will be used.

The equation developed for the thermal conductivity will be a function of two state variables, the intragranular porosity p and the GB coverage X^c_{GB}, obtained from

$$p = N_a G_{grain} \frac{l_c^3}{4} \tag{13}$$

$$X^c_{GB} = \frac{3k_bT}{4(2\gamma + rP_{EXT})f(\theta)} N_{GB}, \tag{14}$$

where G_{grain} is the molar fission gas density within the grain, N_{GB} is the number of gas atoms per unit GB area, $l_c = 0.545$ nm is the lattice constant of UO_2 (Govers et al., 2007), and N_a is Avagadro's number. In addition, γ is the surface tension of the bubbles, r is the bubble radius, k_b is the Boltzmann constant, P_{EXT} is the hydrostatic pressure within the fuel, T is the temperature and $f(\theta)$ is a bubble shape factor. The shape factor is a function of the contact angle θ between the bubble and the GB according to

$$f(\theta) = \frac{1 - 3/2\cos\theta + 1/2\cos^3\theta}{\sin^2\theta}. \tag{15}$$

The value for the bubble radius and surface tension are assumed to be constant and set to $r = 500$ nm and $\gamma = 0.626$ J/m^2.

To determine the thermal conductivity as a function of p and X^c_{GB}, the expression from (Chockalingam et al., 2012a), which takes the form of multipliers to the unirradiated fuel thermal conductivity k_0, i.e. $k = \kappa_{int}\kappa_{GB}k_0$ is used. The multiplier for intragranular porosity κ_{int} is the traditional Maxwell-Eucken formula (Winter and MacInnes, 1988)

$$\kappa_{int} = \frac{1-p}{1+(s-1)p}., \tag{16}$$

where s is a shape parameter, and is set to 0.5 in this work for spherical pores. The multiplier for GB porosity is (Kapitza, 1941)

$$\kappa_{GB} = \frac{1}{1 + k_0 R'_k(X^c_{GB})/d} \tag{17}$$

where $R'_k(X^c_{GB})$ is the effective GB thermal resistance as a function of the GB coverage of bubbles and d is the grain size. An expression for $R'_k(X^c_{GB})$ was developed using atomistic and mesoscale modeling.

A mechanistic description of the impact of GB coverage on the GB thermal resistance in UO_2 was developed using a multiscale approach. The GB and bubble system can be considered as two thermal resistors in parallel, with the effective thermal resistance of the system R'_k equal to

$$\frac{1}{R'_k} = \frac{1}{A_{GB} + A_{bub}} \left(\frac{A_{GB}}{R_k} + \frac{A_{bub}}{R_{bub}} \right), \tag{18}$$

where the area of the bubbles is approximated as $A_{bub} = 2.0 d_{bub} X^c_{GB}$ and the area of influence of the GB as $A_{GB} = d_{GB}(1 - X^c_{GB})$. d_{bub} is the bubble diameter and k_{bub} is the thermal conductivity of the bubbles ($k = 0.00565$ (Thornton, 1960)). d_{GB} is the influence distance perpendicular to the GB.

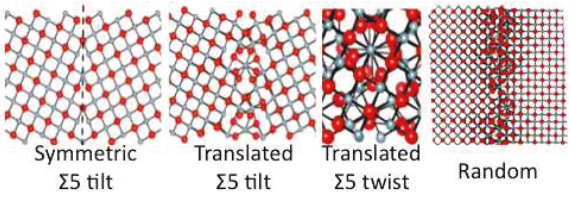

Figure 10: Close-up views of the GB types used in the MD bicrystal simulations to determine the GB thermal resistances.

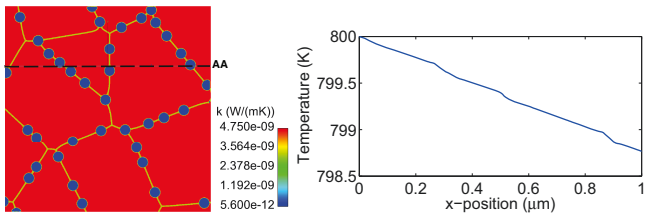

(a) (b)

Figure 11: Mesoscale heat conduction simulations, where (a) shows an example of the polycrystal microstructure for the bicrystal shaded by thermal conductivity and (b) is a plot of the temperature vs x-position along line AA (labeled in (a)).

Note, a detailed derivation of these equations can be found in Tonks et al. (2013a).

MD simulations were used to determine the the thermal resistance of four critical GBs in UO_2, which are shown in Figure 10. The values are shown in Table 4. The Σ5 symmetric tilt boundary has the largest R_k, followed by the random and the Σ5 translated twist boundary, and the Σ5 translated tilt boundary has the smallest.

Values for d_{GB} that correspond to the GB resistances R_k calculated with MD were calculated using a series of 2D heat conduction simulations of a seven grain polycrystal structure with various densities of bubbles and are summarized in detail in (Tonks et al., 2013a). The seven grain polycrystal (generated with a Voronoi tessellation) is 1.0 μm square with an average grain size $d = 0.38$ μm (see Figure 11(a)). Note that the grain sizes are significantly smaller than those typically found in UO_2 fuel ($d \sim 10$ μm). However, previous publications have shown that the effective GB resistance computed from mesoscale simulations is independent of the grain size used in the simulations (Millett and Tonks, 2011; Chockalingam et al., 2012a). The effective GB thermal resistance vs GB coverage X^c_{GB} is shown in Figure 12 for all the mesoscale simulations.

Table 4: Kapitza resistance for four types of GBs in UO_2 calculated using MD simulation at three different temperatures.

	R_k ($\times 10^{-9}$ m^2 K/W)		
GB type	300 K	800 K	1500 K
Σ5 sym. tilt	1.69	1.14	0.92
Σ5 tr. tilt	1.08	0.83	0.60
Σ5 tr. twist	1.38	0.86	0.63
Random	1.48	0.97	0.66

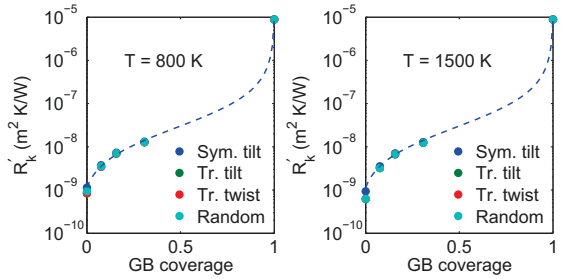

Figure 12: The effect of GB coverage on the effective GB thermal resistance using the MD-determined values for the GB thermal resistance. Note that the GB type has little effect on the effective GB thermal resistance at both 800 and 1500 K.

The values for d_{GB} for various values of R_k are determined by fitting the effective thermal resistance model to the results from the mesoscale simulations. The predictions from the model compare well to the simulation data, as shown in Figure 12. The model also captures the extreme cases when $X^c_{GB} = 0$ (a clean GB) and when $X^c_{GB} = 1.0$ (only bubble with no visible GB). Additional simulations have also shown that the model accurately predicts the impact of intergranular bubbles of various radii. From the simulations, it is clear that the type of GB does not have a significant impact on the values of the effective GB thermal resistance, using the values for both $T = 800$ and 1500 K (Figure 12). Thus, it was found that the model predictions with $d_{GB} = 4.0$ nm compared well with the simulation data for all GB types.

This multiscale thermal conductivity model was implemented in BISON and applied in a series of macroscale simulations. These simulations employed the various material models for the fuel and cladding behavior from the literature described above, with three changes. First, the boundary condition on the outside of the cladding is determined using a simple coolant channel model. Second, the power profile within the fuel varies with position, as determined by the model of (Lassmann et al., 1994). Finally, it was assumed that percolated GB bubbles do not close after fission gas release, such that the GB coverage stops evolving and maintains the percolation value. In addition, in order to implement this multiscale model, the fuel thermal conductivity model (Lucuta et al., 1996) was modified such that the fission gas is accounted for with a multiscale fission gas thermal conductivity model (Eqs. (16) and (17)) rather than the porosity multiplier. Thus, the degradation of the thermal conductivity due to all radiation damage besides fission gas is still accounted for by that model.

For these simulations, the behavior of a 10-pellet rodlet with a 10 micron average grain size under typical PWR conditions is predicted during two years in the reactor. The rodlet geometry is represented in 2D by taking advantage of axisymmetry, as shown in Figure 13(a). For each example shown in this section, the simulation results are compared to those from an identical simulation, except that the contribution of the fission gas to the thermal conductivity from the multiscale model was set to zero. Thus, by comparing the two simulation results the impact of

this model on the thermal conductivity and the temperature can be easily observed.

Evolution of the two state variables with time is plotted at two locations within the fuel rodlet, labeled as 1 and 2 in Figure 13(a). Values of the state variables over time at the center of the pellet (point 1) are shown in Figure 13(b). At point 1, the GB coverage steadily increases until it reaches the percolation threshold and fission gas begins to be released into the gap and plenum. The intragranular porosity steadily increases throughout the simulation.

To demonstrate the effect of the state variable evolution, the difference between the thermal conductivity predicted by the multiscale model and the thermal conductivity in the reference case at point 1 is plotted in Figure 13(c), as is the difference between the temperatures. The impact of the multiscale model on the thermal conductivity is dominated by the grain boundary bubbles, with the intragranular porosity only having a small effect. The thermal conductivity decreases from the reference case until the GB coverage reaches the percolation threshold, at which time the value stays fairly constant. Temperature steadily increases from the reference case, even beyond when the GB coverage reaches the percolation threshold. This is because the local temperature is impacted by the thermal conductivity in the surrounding material as well as at the local point.

At point 2, on the outer edge of the pellet (see Figure 13(a)), the GB coverage increases much slower than at point 1, due to the lower temperature and thus lower gas diffusivity, as shown in Figure 13(d). Since the fission gas cannot diffuse as rapidly to the GB, more of the gas is trapped in the grain interior and thus the intragranular porosity increases at nearly twice the rate of point 1. Both the intragranular porosity and the GB coverage impact the thermal conductivity and the temperature (see Figure 13(e)), though the intragranular fission gas now has the larger impact.

6. Conclusions

Perhaps no field of computational science is a better example of the need for multiphysics coupling than nuclear fuel performance modeling. The fundamental transfer of heat from fuel pellets, across a gas-filled gap, and through cladding into the coolant is a multiphysics problem that poses numerical challenges. When the equations of solid mechanics and heat transfer are closely intertwined, as in the case just described, it is advantageous to solve the equations in a tightly coupled fashion through a technique such as JFNK.

While the input to a nuclear fuel performance code typically includes a power history, it is possible to couple the performance code to a neutronics code that supplies a fission density. This has been done by coupling BISON to DeCART. Care must be taken in the manner by which the fission density is mapped to the fuel performance code in order to preserve the overall pin power. Additionally, it is important to consider the mesh density used in the two physics solvers to ensure that the transfer results in satisfactorily smooth data. This coupling also allows the temperature computed by the fuel performance code to affect the neutronics calculation through the temperature's influence on cross sections.

Multiscale coupling is the last form of multiphysics coupling discussed here. One variety of multiscale coupling is a concurrent approach wherein lower length scale calculations inform higher length scale results, and vice versa, during the calculation. For example, evolving microstructure results in changing thermal conductivity, which is used at the macroscale. The changing temperature at the macroscale in turn affects grain growth and bubble history at the microscale. By coupling BISON and MARMOT, it is possible to study these relationships.

A second variety of multiscale coupling is a hierarchical approach. With this approach, lower lengthscale simulations are conducted separately to inform an analytical model that accounts for the lower lengthscale physics.

In addition to these techniques, many other options are possible. For example, BISON and MARMOT have also been coupled to a thermal hydraulics code, a neutronics code, and a CRUD-formation code to simulate CRUD-induced power shift (Gaston et al., 2014). As these examples show, advances in computing power and software development are enabling first-of-their-kind analyses of nuclear systems. These advances are beginning to make it possible to study the interaction of many connected phenomena from first principles.

Acknowledgments

We would like to thank Dr. Tomas J. Downar, Dr. Benjamin Collins, and Michael Rose at the University of Michigan for their help with the neutronics coupling. The submitted manuscript has been authored by a contractor of the U.S. Government under Contract DE-AC07-05ID14517. Accordingly, the U.S. Government retains a non-exclusive, royalty-free license to publish or reproduce the published form of this contribution, or allow others to do so, for U.S. Government purposes.

References

Allison, C. M., Berna, G. A., Chambers, R., Coryell, E. W., Davis, K. L., Hagrman, D. L., Hagrman, D. T., Hampton, N. L., Hohorst, J. K., Mason, R. E., McComas, M. L., McNeil, K. A., Miller, R. L., Olsen, C. S., Reymann, G. A., Siefken, L. J., 1993. SCDAP/RELAP5/MOD3.1 code manual, volume IV: MATPRO–A library of materials properties for light-water-reactor accident analysis. Tech. Rep. NUREG/CR-6150, EGG-2720, Idaho National Engineering Laboratory.

Carlson, N. N., Unal, C., Galloway, J. D., 2013. Formulation of the constituent distribution model implemented into the BISON framework for the analysis of performance of metallic fuels with some initial simulation results. Tech. Rep. LA-UR-13-26824, Los Alamos National Laboratory.

Chockalingam, K., Millett, P., Tonks, M., 2012a. Effects of intergranular gas bubbles on thermal conductivity. J. Nucl. Mater. 430, 166–170.

Chockalingam, K., Tonks, M. R., Hales, J. D., Gaston, D. R., Millett, P. C., Zhang, L., 2012b. Crystal plasticity with Jacobian-free Newton–Krylov. Computational Mechanics, 1–11.

Dowling, D., White, R., Tucker, M., 1982. The effect of irradiation-induced re-solution on fission gas release. J. Nucl. Mater. 110 (1), 37–46.

Fink, J. K., 2000. Thermophysical properties of uranium dioxide. J. Nucl Materials 279 (1), 1–18.

Forsberg, K., Massih, A. R., 1985. Diffusion theory of fission gas migration in irradiated nuclear fuel UO_2. J. Nucl Materials 135 (2-3), 140–148.

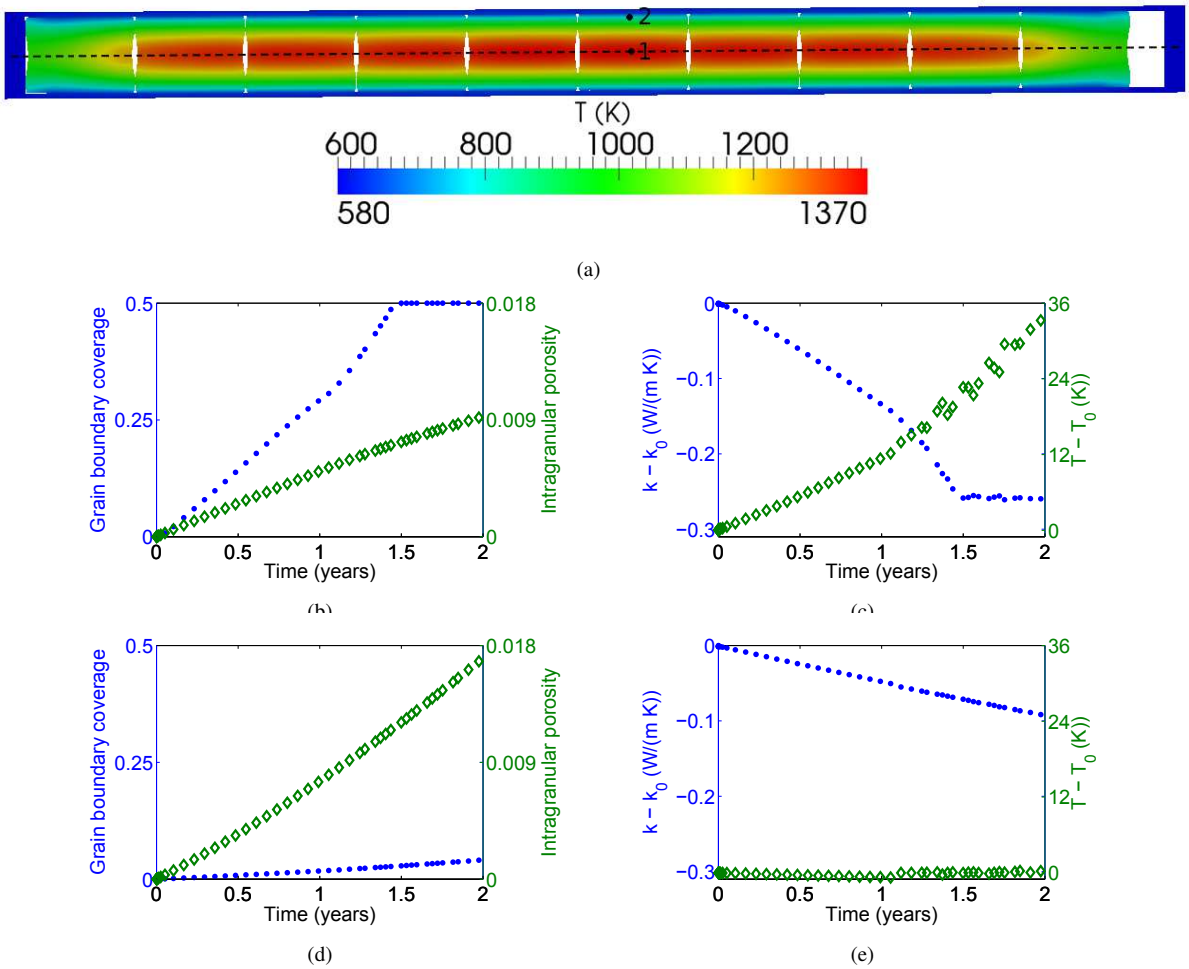

Figure 13: Results from the 10-pellet rodlet simulation using the multiscale model of thermal conductivity, where (a) shows the rodlet with the RZ domain mirrored at the center line, (b) and (d) plot the GB coverage and intragranular porosity at points 1 and 2, respectively (labeled in (a)) while (c) and (e) plot the change in the thermal conductivity and in the temperature over time, compared to the thermal conductivity k_0 and temperature T_0 from the reference case, at points 1 and 2, respectively.

Gaston, D., Newman, C., Hansen, G., Lebrun-Grandié, D., 2009. MOOSE: A parallel computational framework for coupled systems of nonlinear equations. Nucl. Eng. Design 239, 1768–1778.
URL http://dx.doi.org/10.1016/j.nucengdes.2009.05.021

Gaston, D. R., Permann, C. J., Peterson, J. W., Slaughter, A. E., Andrš, D., Wang, Y., Short, M. P., Perez, D. M., Tonks, M. R., Ortensi, J., Martineau, R. C., 2014. Physics-based multiscale coupling for full core nuclear reactor simulation. Ann. Nuclear EnergyUnder review.

Gould, I., Hermann, O. W., Westfall, R. M., 2009. Origen-s: Scale system module to calculate fuel depletion, actinide transmutation, fission product buildup and decay, and associated radiation source terms. Tech. Rep. ORNL/TM-2005/39, Oak Ridge National Laboratory.

Govers, K., Lemehov, S., Hou, M., Verwerft, M., 2007. Comparison of interatomic potentials for uo2. part i: Static calculations. J. Nucl Materials 366 (1-2), 161 – 177.

Hales, J. D., Novascone, S. R., Williamson, R. L., Gaston, D. R., Tonks, M. R., 2012. Solving nonlinear solid mechanics problems with the Jacobian-free Newton Krylov method. CMES: Comput. Model. Eng. Sci. 84 (2), 123–154.

Hales, J. D., Williamson, R. L., Novascone, S. R., Perez, D. M., Spencer, B. W., Pastore, G., 2013. Multidimensional multiphysics simulation of TRISO particle fuel. J. Nucl. Mater. 443, 531–543.
URL http://dx.doi.org/10.1016/j.jnucmat.2013.07.070

Hamilton, S., Clarno, K., 2011. Mathematical framework for the coupling of AMP and Denovo codes. In: Transactions of the American Nuclear Society. Vol. 105. ANS, pp. 515–517.

Hamilton, S., Clarno, K., Philip, B., Berrill, M., Ampath, R., Allu, S., 2012. Integrated radiation transport and nuclear fuel performance for assembly-level simulations. In: PHYSOR 2012 Advances in Reactor Physics Linking Research Industry and Education. ANS, knoxvill, Tenessee USA, April 15 - 20.

Hu, S., Henager Jr, C. H., 2009. Phase-field modeling of void lattice formation under irradiation. Journal of Nuclear Materials 394 (2), 155–159.

Hu, S., Jr., C. H., Heinisch, H. L., Stan, M., Baskes, M. I., Valone, S. M., 2009. Phase-field modeling of gas bubbles and thermal conductivity evolution in nuclear fuels. J. Nucl. Mater. 392 (2), 292 – 300.

Hursin, M., Downar, T. J., Montgomery, R., 2013. Impact of improved neutronic methodology on the cladding response during a PWR reactivity initiated accident. Nuclear Engineering and Design 262, 180 – 188.

Joo, H. G., Cho, J. Y., Kim, K. S., Lee, C. C., Zee, S. Q., Apr. 25–29, 2004. Methods and performance of a three-dimensional whole-core transport code DeCART. In: PHYSOR 2004 – The Physics of Fuel Cycles and Advanced Nuclear Systems: Global Developments, Chicago, Illinois. American Nuclear Society.
URL http://hdl.handle.net/10371/9630

Joo, H. G., Cho, J. Y., Kim, K. S., Zee, S. Q., Chang, M. H., 2002. Dynamic implementation of the equivalance theory in the heterogeneous whole core transport calculation. In: PHYSOR 2002 International Conference on the New Frontiers of Nuclear Technology: Reactor Physics Saftey and High Performance Computing. ANS, pp. 1–13, seoul, Korea, Octorber 7 - 10.

Kapitza, P., 1941. J. Phys. (Moscow) 4, 181.

Kelly, B. W., Collins, B., Larsen, E. W., 2013. 2D/1D approximations to the 3D neutron transport equation. II:numerical comparisons. In: International Conference on Mathematics and Computational Methods Applied to Nuclear Science and Engineering. ANS, pp. 1358–1368, sun Valley, Idaho, May 5 - 9.

Kelly, B. W., Larsen, E. W., 2013. 2D/1D approximations to the 3D neutron transport equation. I:theory. In: International Conference on Mathematics and Computational Methods Applied to Nuclear Science and Engineering. ANS, pp. 1346–1357, sun Valley, Idaho, May 5 - 9.

Knoll, D. A., Keyes, D. E., 2004. Jacobian-free Newton-Krylov methods: a survey of approaches and applications. J. Comput. Phys. 193 (2), 357–397.

Lassmann, K., O'Carroll, C., van de Laar, J., Walker, C. T., 1994. The radial distribution of plutonium in high burnup UO_2 fuels. J. Nucl. Materials 208, 223–231.

Lee, C. B., Kim, D. H., Song, J. S., Bang, J. G., Jung, Y. H., 2000. RAPID model to predict radial burnup distribution in LWR UO_2 fuel. Journal of Nuclear Materials 282 (1), 196 – 204.

Lemehov, S., Nakamura, J., Suzuki, M., 2001. Pluton: a three group model for the radial distribution of plutonium, burnup, and power profiles in highly irradiated LWR fuel rods. Nuclear Technology 133, 153 – 168.

Lewis, E. E., Miller, W. F., 1984. Computational Methods of Neutron Transport. John Wiley & Sons.

Lucuta, P. G., Matzke, H. J., Hastings, I. J., 1996. A pragmatic approach to modelling thermal conductivity of irradiated UO_2 fuel: review and recommendations. J. Nucl. Mater. 232, 166–180.

Medvedev, P., 2012. Fuel performance modeling results for representative FCRD irradiation experiments: Projected deformation in the annular AFC-3A U-10Zr fuel pins and comparison to alternative designs. Tech. Rep. INL/EXT-12-27183 Revision 1, Idaho National Laboratory.

Medvedev, P., 2013. Summary report on the fuel performance modeling of the AFC-2A, 2B irradiation experiments. Tech. Rep. INL/EXT-13-30006, Idaho National Laboratory.

Metzger, K. E., Knight, T. W., Williamson, R. L., April 6–9 2014. Model of U_3Si_2 fuel system using BISON fuel code. In: Proceedings of the International Congress on Advances in Nuclear Power Plants - ICAPP 2014. Charlotte, NC.

Millett, P., M., T., 2010. Application of phase-field modeling to irradiation effects in materials. Current Opinion Solid State and Mat. Sci. doi:10.1016/j.cossms.2010.10.002.

Millett, P. C., El-Azab, A., Rokkam, S., Tonks, M., Wolf, D., 2011a. Phase-field simulation of irradiated metals: Part i: Void kinetics. Computational Materials Science 50 (3), 949–959.

Millett, P. C., El-Azab, A., Wolf, D., 2011b. Phase-field simulation of irradiated metals: Part ii: Gas bubble kinetics. Computational Materials Science 50 (3), 960–970.

Millett, P. C., Tonks, M., 2011. Meso-scale modeling of the influence of intergranular gas bubbles on effective thermal conductivity. J. Nucl. Mater. 412 (3), 281 – 286.

Millett, P. C., Tonks, M. R., Chockalingam, K., Zhang, Y., Biner, S., 2013. Three dimensional calculations of the effective kapitza resistance of UO_2 grain boundaries containing intergranular bubbles. Journal of Nuclear Materials 439 (1), 117–122.

Novascone, S. R., Spencer, B. W., Andrs, D., Williamson, R. L., Hales, J. D., Perez, D. M., May 5-9, 2013. Results from tight and loose coupled multiphysics in nuclear fuels performance simulations using BISON. In: Proceedings of the International Conference on Mathematics and Computational Methods Applied to Nuclear Science and Engineering. Sun Valley, Idaho.

Olander, D. R., 1976. Fundamental aspects of nuclear reactor fuel elements. Technical Information Center, Energy Research and Development Administration.

Pastore, G., Luzzi, L., Di Marcello, V., Van Uffelen, P., 2013. Physics-based modelling of fission gas swelling and release in UO_2 applied to integral fuel rod analysis. Nuclear Engineering and Design 256, 75–86.

Rashid, J., Yagnik, S., Montgomery, R., 2011. Light water reactor fuel performance modeling and multi-dimensional simulation. JOM-J Min Met Mat S 63 (8), 81–88.

Ross, A. M., Stoute, R. L., 1962. Heat transfer coefficient between UO_2 and Zircaloy-2. Tech. Rep. AECL-1552, Atomic Energy of Canada Limited.

Saad, Y., Schultz, M. H., 1986. GMRES: a generalized minimal residual algorithm for solving linear systems. SIAM J. Sci. Statist. Comput. 7, 856.

Soba, A., Denis, A., Romero, L., Villarino, E., Sardella, F., 2013. A high burnup model developed for the DIONISIO code. Journal of Nuclear Materials 433, 160–166.

Thornton, E., 1960. Viscosity and thermal conductivity of binary gas mixtures: Xenon-krypton, xenon-argon, xenon-neon and xenon-helium. Proceedings of the Physical Society 76 (1), 104.
URL http://stacks.iop.org/0370-1328/76/i=1/a=313

Tonks, M., Gaston, D., Millett, P., Andrs, D., Talbot, P., 2012. An object-oriented finite element framework for multiphysics phase field simulations. Comp. Mat. Sci. 51 (1), 20–29.

Tonks, M., Gaston, D., Permann, C., Millett, P., Hansen, G., Wolf, D., 2010. A coupling methodology for mesoscale-informed nuclear fuel performance codes. Nucl. Eng. Design 240, 2877–83.

Tonks, M. R., Millett, P. C., Nerikar, P., Du, S., Andersson, D., Stanek, C. R., Gaston, D., Andrs, D., Williamson, R., 2013a. Multiscale development of a fission gas thermal conductivity model: Coupling atomic, meso and continuum level simulations. Journal of Nuclear Materials 440 (1), 193–200.

Tonks, M. R., Zhang, Y., Bai, X., Millett, P. C., 2014. Demonstrating the temperature gradient impact on grain growth in UO_2 using the phase field method. Materials Research Letters 2 (1), 23–28.

Tonks, M. R., Zhang, Y., Biner, S., Millett, P. C., Bai, X., 2013b. Guidance to design grain boundary mobility experiments with molecular dynamics and phase-field modeling. Acta Materialia 61, 1373–1382.

Williamson, R. L., Hales, J. D., Novascone, S. R., Tonks, M. R., Gaston, D. R., Permann, C. J., Andrs, D., Martineau, R. C., 2012. Multidimensional multiphysics simulation of nuclear fuel behavior. J. Nucl. Mater. 423, 149–163.
URL http://dx.doi.org/10.1016/j.jnucmat.2012.01.012

Winter, P., MacInnes, D., 18-20 Sept 1988. IAEA technical committee on water reactor fuel element computer modelling in steady-state, transient and accident conditions. Preston, UK, Paper No. IAEA-TC-657/5.6.

Zhang, L., Tonks, M., Millett, P., Zhang, Y., Chockalingam, K., Biner, B., 2012a. Phase-field modeling of temperature gradient driven pore migration coupling with thermal conduction. Computational Materials Science.

Zhang, L., Tonks, M. R., Gaston, D., Peterson, J. W., Andrs, D., Millett, P. C., Biner, B. S., 2012b. A quantitative comparison between c0 and c1 elements for solving the Cahn-Hilliard equation. Journal of Computational Physics.